Hindawi
Shock and Vibration
Volume 2018, Article ID 9501746, 15 pages
https://doi.org/10.1155/2018/9501746

Research Article

Dynamic Response of a Combined Isolation Based Mega-Substructure under Bidirectional Near-Fault Ground Motions

Xueyuan Yan, Weihong Chen, Shen Shi, and Xuan Wang

College of Civil Engineering, Fuzhou University, Fuzhou 350116, China

Correspondence should be addressed to Weihong Chen; chenweihong1980@163.com

Received 13 June 2018; Accepted 25 September 2018; Published 1 November 2018

Academic Editor: Angelo Marcelo Tusset

A typical megaframe structure has a high lateral stiffness and is excellent for high-rise structures. However, this high stiffness can lead to poor seismic response of a structure. Seismic isolation technology is a mature and cheap vibration control method that is used for vibration reduction in megaframes. This paper introduces a megaframe structure based on substructure combined isolation. The structure consists of two parts. The main body is a megaframe, and the substructure is the subframe with the combined isolation layer arranged at the bottom of the subframe. The seismic performance of this structure system was evaluated by performing shaking table tests of two megaframe model structures. The responses of the deformation, acceleration, and shear of the structure were measured. The dynamic behaviors of the structure with or without the combined isolation layer when exposed to single and bidirectional near-fault and far-fault ground motions with different peak values were investigated. The results showed that the combined isolation layer can reduce the bidirectional seismic response of the main frame and subframe. The acceleration, base shear, and displacement responses had similar vibration reduction trends for the two model structures, and the structural responses under bidirectional earthquake were generally greater than that under a single directional earthquake. The near-fault pulse effect increased the seismic response of the structure. The increase of the predominant period of ground motion also increased the seismic response of the structure.

1. Introduction

Currently, there are hundreds of super high-rise buildings built every year in the world. Super high-rise buildings can adopt different structural systems. The megaframe structure system is one of the most used structure systems for these super high-rises. The megaframe structure system is a two-stage stress system. The external megabeam and column have a large cross section and lateral stiffness. The internal substructure adopts a conventional size and has a small lateral stiffness. Brunesi et al. [1] and Lu et al. [2, 3] studied the performance of megaframe structural systems through numerical analysis and shaking table tests. The seismic properties of a hybrid high-rise structure that had two structural systems were studied by shaking table test and numerical analysis [4]. The progressive collapse-resisting capacity of modular mega-frame structures consisting of a few identical subsystems was investigated based on a column-loss scenario [5].

Seismic isolation technology is a mature and cheap vibration control technique, and one of the typical forms is combined isolation. A residential building was retrofitted by using a hybrid base isolation system, and five free vibration tests were carried out [6]. A hybrid friction-controllable sliding system for seismic response control of buildings was introduced [7]. Experimental and analytical results for the seismic response of a rigid structure supported on hybrid isolation systems were presented by Chang et al. [8]. A constrained optimization procedure for the dynamic analysis of hybrid base isolation systems under earthquake excitation was present by Oliveto et al. [9]. The seismic response of isolated structures under bidirectional

earthquakes was investigated [10–13]. The response of isolated structures under near-fault earthquakes has seen significant research in recent years. The disorder and damage of appliances in the operation room under near-fault ground motion and long-period ground motion were recorded during shaking table tests [14]. Numerical analyses of base-isolated buildings under near-fault ground motions were performed [15–19]. Responses of the isolated building based on a shape-memory-alloy supplemented rubber bearing were evaluated by dynamic time-history analysis under a set of recorded, near-fault, and fault-normal components of ground motions [20]. The efficiency of active control systems in reducing the responses of base-isolated structures with various isolation parameters under near-fault earthquake was investigated [21].

The isolation technique can be applied to the substructure of the megaframe structure system to improve the ability of the megaframe structural system to resist earthquakes. Feng et al. [22, 23] proposed a mega-substructure vibration control system and studied its dynamic characteristics and dynamic parameters optimization. Following Feng's work, some scholars have successively carried out related research on applying vibration control technology to the megaframe structure system. Shaking table tests of a normal reinforced concrete megaframe structure and a multifunctional vibration-absorption reinforced concrete megaframe structure were performed, and the dynamic characteristics, the seismic responses, and the failure mechanism of these two models under earthquake motions were studied [24]. Passive mega-substructure-controlled structures were presented, and a parametric study of their structural characteristics was performed [25–27]. A mega-substructure isolation system was developed, and shaking table tests of the isolated structure, lower substructure-consolidated structure, and the aseismic structure were carried out. The equations of motion of the mega-subisolation structure were established, and then numerical analysis results were compared to the tests [28, 29].

The literature as summarized above represents significant progress. However, there is less research on megaframes with different forms of seismic isolation. Therefore, this study investigates a megaframe structure system with a combined isolation layer at the bottom of the substructure. Two model structures were studied by shaking table test to obtain the actual vibration-absorbing performance of this structural system. The first model was one where the bottom of the substructure was consolidated with a megaframe, and the second was a system with the combined isolation layer at the bottom of the substructure. The dynamic responses of the two different systems under different ground motions with different seismic intensity in one direction and two directions were studied to investigate the entire behavior of the structural system.

2. Methodology

2.1. Test Models. The test was conducted using the earthquake simulation shaking table system of Fuzhou University. The model was a three-story steel-frame megastructure. Three subframes can be arranged in the setup. Labeled from the bottom to the top, these subframes are the first subframe, second subframe, and third subframe. For this study, there was a requirement of a large space at the bottom of the structure, so the first subframe was not set in this experimental model. The subframes were reduced from the original 6 layers to 3 layers, and the 5×6 spans were simplified to 2×3 spans to facilitate the manufacturing of test models and the placement of weights and sensors. The structure model was 1.6 m long, 1.0 m wide, and 3.27 m high, and the mega-column was 140×10 angle steel, the mega main beam was 12.6# channel steel, the mega secondary beam was 8# channel steel, the secondary frame column was $60 \times 60 \times 2.5$ square steel, and the subframe beam used $40 \times 40 \times 1.5$ square steel. The weight of the model structure was 1.851 t, the counterweight of each floor of the main frame was 0.28 t, the counterweight of each floor of subframes was 0.55 t, and the total weight of the model was 5.991 t. A 15 mm wide isolation joint was arranged between the subframe and the outer main frame. In the combined isolation of the subframes, two lead rubber bearings and two elastic sliding bearings were installed at the connection of each subframe and the main frame. A photo of the model and its schematics are shown in Figure 1. The mechanical properties from testing and geometric parameters of the isolation bearings are given in Table 1.

2.2. Experimental Method

2.2.1. Measurements. The dynamic response of the structural system was accurately measured by acceleration sensors and displacement sensors that were arranged on the model as shown in Figure 2. An acceleration sensor was placed along both the X-direction and Y-direction on the shaking table to measure the actual input of the system. For the outer main frame and the inner subframe, one acceleration sensor was arranged along both the X-direction and Y-direction for each floor of the outer main frame and for the two subframes to obtain the acceleration response. The arrangement of the acceleration sensor is the same for the aseismic structure and the isolated structure. The measurement of the displacement response of the aseismic structure model was done with one displacement sensor placed along both the X-direction and Y-direction in the middle of each floor's main beam of the outer main frame, and one displacement sensor arranged along both the X-direction and Y-direction at the top of the subframe. For the isolated structure, one displacement sensor was set on the isolation layer of the substructure along the X-direction and Y-direction. In addition, to measure the force reaction of the four columns of the main frame, four three-dimension force sensors were arranged at the junction between the columns and the shaking table. The upper connecting plate of the three-dimension force sensor was connected with the structure model, and the bottom plate was connected with the shaking table.

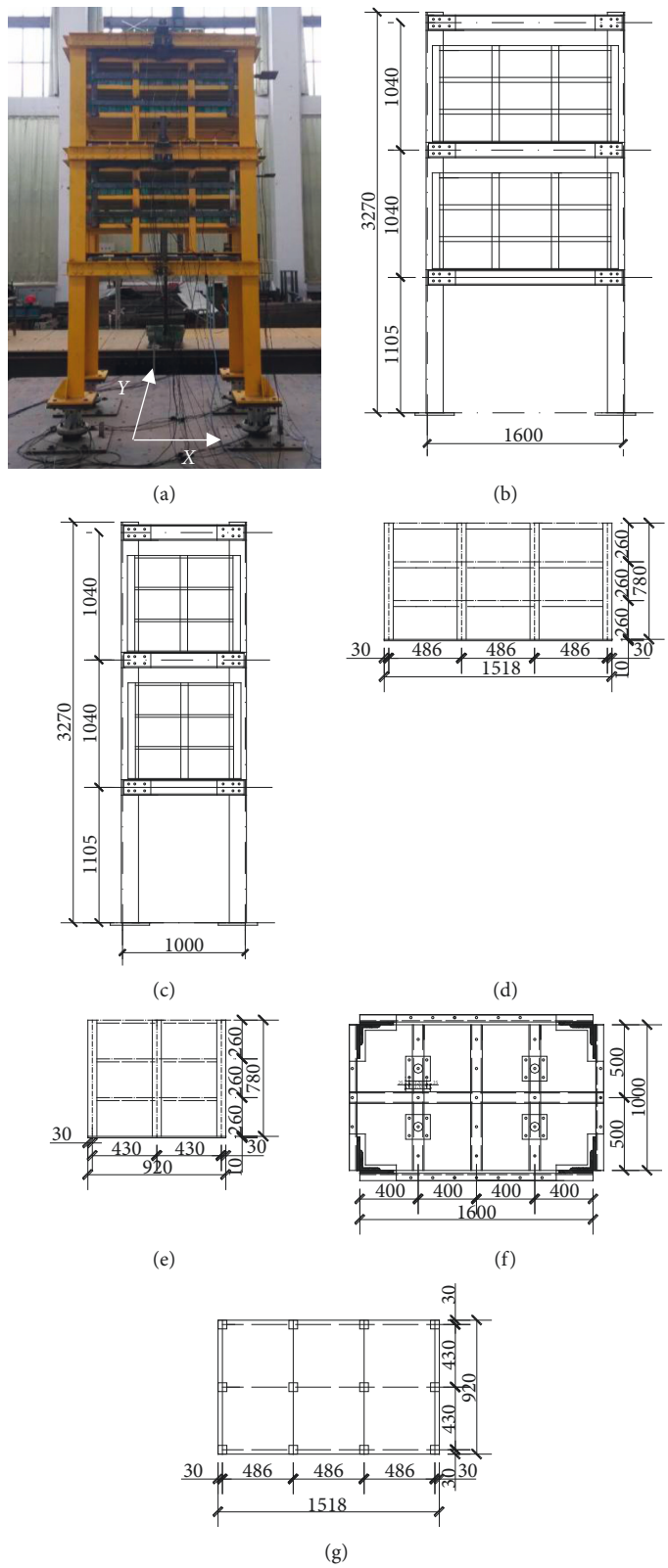

FIGURE 1: Mega-substructure model. (a) Picture of the mega-substructure, (b) front elevation of the mega-substructure, (c) side elevation of the mega-substructure, (d) front elevation of the subframe, (e) side elevation of the subframe, (f) plan of the main frame, and (g) plan of the subframe.

Table 1: Isolation bearing parameters.

Parameter	Shear modulus	Overall height	External diameter	Diameter of lead	Total height of rubber	Total height of steel plate	Horizontal stiffness	Vertical stiffness	Horizontal stiffness (elastic sliding)	Friction coefficient (elastic sliding)
Unit	MPa	mm	mm	mm	mm	mm	N/mm	kN/mm	N/mm	—
Value	0.392	35	65	10	7(6)	2.0 × 4(3)	145.1 (164.7)	22.5 (19.3)	134.1 (149.8)	0.04

Note. The values in brackets represent the relevant parameters of the third subframe isolation bearings, and the rest are the common parameters of the second and third subframe isolation bearings.

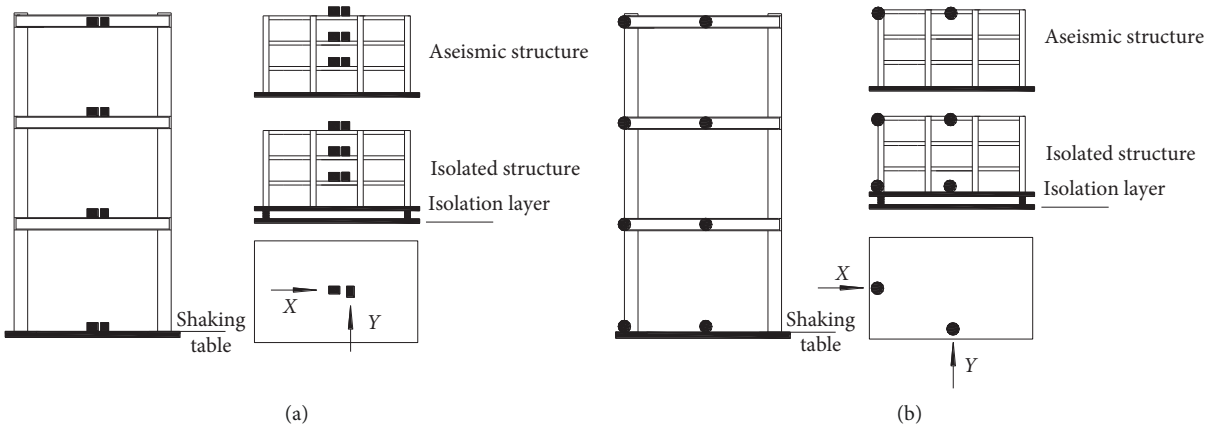

Figure 2: Sensor layout: (a) acceleration sensor; (b) displacement sensor.

2.2.2. Ground Motion Input. Three records from different stations of the Chi-Chi earthquake were selected as inputs for the shaking table test to study the dynamic responses of the structures under near-fault and far-fault ground motion. The specific parameters of the ground motions are shown in Table 2.

Shaking table test cases of the model structures are shown in Table 3. White noise tests were performed on the structure models first to acquire the vibration periods of the model structures. The differences in dynamic responses of the structure models under single-directional and bidirectional inputs of ground motion were studied using two horizontal components of the ground motion records. For the bidirectional input, the records' W-E component was applied to the *Y*-direction, and the N-S component was the input to the *X*-direction. The amplitude of the two components applied was amplitude-modulated in proportion to the actual seismic record. The input amplitudes were divided into 3 levels corresponding to a 7-degree frequent earthquake, 7-degree design earthquake, and 7-degree rare earthquake. There were 16 test cases performed on the mega-substructure based on substructure combined isolation (hereinafter referred to as "combined isolation structure"). After testing, the isolation layers were disassembled, and the bottom of the substructures was fixed to the megaframe. Then, the test cases for the aseismic mega-substructure (hereinafter referred to as "aseismic structure") were performed. There were also 16 tests performed on the aseismic structure. White noise tests were again performed after each case.

3. Results and Discussion

The basic periods of the aseismic structure and the combined isolated structure obtained by the white noise test were 0.463 s and 0.501 s, respectively. The result shows that the basic period of the combined isolation structure is not significantly longer than the aseismic structure. Since the combined isolation layer is arranged at the joint of the subframe and the main frame. This is different from the isolation layer set at the bottom of the foundation, and the megastructure itself has a longer period.

3.1. Subframe Seismic Response. For the following discussion, the damping rate α is defined as $\alpha = ((R_a - R_{is})/R_a) \times 100\%$, where R_a is the seismic response of the aseismic structure and R_{is} is the seismic response of the combined isolation structure.

3.1.1. Subframe Acceleration Response. Table 4 shows the acceleration response and damping rate for each floor of the subframe in the aseismic structure and the combined isolation structure for every test case. Figures 3 and 4 shows the *X*-axis and *Y*-axis acceleration response time histories and comparisons of the top floor of the third subframe of the aseismic structure and the combined isolation structure, respectively, for cases B6, B7, and B8. From the table and figures, it can be seen that the isolation layer has a significant damping effect for the structural acceleration response of the

Table 2: Earthquakes records used for test inputs.

Earthquake name	Station	Site	Type	Fault distance (km)	Component	PGA (gal)	PGV (cm/s)	PGV/PGA (s)
Chi-Chi-2N	TCU056	Class II	Near-fault	10.48	WE	153.23	42.86	0.28
					NS	140.14	39.54	0.28
Chi-Chi-2F	TAP042	Class II	Far-fault	106.48	WE	94.91	12.34	0.13
					NS	86.33	7.77	0.09
Chi-Chi-3N	TCU110	Class III	Near-fault	11.58	WE	187.96	48.72	0.26
					NS	176.69	56.56	0.32

Note. Earthquake name suffixes "2, 3" indicate "Type II and III sites" and "N, F" indicate "near-faults, far-faults," respectively.

Table 3: Test cases.

No.	Test cases	Input earthquake	Input direction	Input peak (g)	Instructions
1	B0	White noise	*X*, *Y*	\	\
2	S1	Chi-Chi-2N	*Y*	0.056 g	7-degree frequent earthquake
3	S2	Chi-Chi-2F	*Y*	0.056 g	7-degree frequent earthquake
4	B1	Chi-Chi-2N	*X* + *Y*	0.051 g + 0.056 g	7-degree frequent earthquake
5	B2	Chi-Chi-2F	*X* + *Y*	0.051 g + 0.056 g	7-degree frequent earthquake
6	S3	Chi-Chi-2N	*Y*	0.153 g	7-degree design earthquake
7	S4	Chi-Chi-2F	*Y*	0.153 g	7-degree design earthquake
8	S5	Chi-Chi-3N	*Y*	0.153 g	7-degree design earthquake
9	B3	Chi-Chi-2N	*X* + *Y*	0.140 g + 0.153 g	7-degree design earthquake
10	B4	Chi-Chi-2F	*X* + *Y*	0.139 g + 0.153 g	7-degree design earthquake
11	B5	Chi-Chi-3N	*X* + *Y*	0.113 g + 0.153 g	7-degree design earthquake
12	S6	Chi-Chi-2N	*Y*	0.316 g	7-degrees of rare earthquake
13	S7	Chi-Chi-2F	*Y*	0.316 g	7-degrees of rare earthquake
14	S8	Chi-Chi-3N	*Y*	0.316 g	7-degree rare earthquake
15	B6	Chi-Chi-2N	*X* + *Y*	0.289 g + 0.316 g	7-degree rare earthquake
16	B7	Chi-Chi-2F	*X* + *Y*	0.288 g + 0.316 g	7-degree rare earthquake
17	B8	Chi-Chi-3N	*X* + *Y*	0.297 g + 0.316 g	7-degree rare earthquake

Note. The W-E component of Chi-Chi ground motions was used for single-directional inputs. The N-S and W-E components of Chi-Chi ground motions were inputs for the *X*-direction and *Y*-direction, respectively, during bidirectional tests. For the test cases, "S" represents single-directional input and "B" represents bidirectional input.

two subframes in both directions under both the far-fault and near-fault ground motions. The damping rate has a minimum of 32.93% and a maximum of 66.20%. The vibration reduction effects in both directions are similar. In general, the acceleration response of the subframe under the bidirectional earthquake is greater than that under the single-directional earthquake. The acceleration responses of the subframes of the two structural systems increase with the increase of the floor. Also, the acceleration response of each floor of the second subframe is greater than the third subframe. The response difference of each floor of the subframe of the combined isolation structure is smaller than that of the aseismic structure and is close but not completely the same as the horizontal rigid-body movement of the base-isolation structure. As the input amplitude of ground motion increases, the acceleration response of the subframe increases. Due to the influence of the pulse effect, the acceleration response of the subframe under the action of the Chi-Chi-2N ground motion with different intensity is greater than that under the Chi-Chi-2F ground motion for the same site type class II. However, the damping rate is similar for the two ground motions. Under near-fault ground motion, the acceleration response of the subframe is greater than the Chi-Chi-2N ground motion since the predominant period of the Chi-Chi-3N ground motion on the Class III site is closer to the basic period of the structure.

In the mega-substructure system, the subframe serves as the main space for work and life. Thus, structural vibration control is focused on the safety and integrity of the subframe. The ground motion acceleration signal is transmitted from the foundation to the upper structure, amplified by the main frame, and then transmitted to the subframe. When the subframe had the combined isolation layer, the acceleration response of the subframe is smaller than that of the nonisolated case due to the filtering and the energy dissipation of the isolation layer. In a formal and mechanical sense, the isolated subframe itself is similar to a base-isolated structure.

3.1.2. Subframe Displacement Response. Table 5 shows the displacement responses and damping rate of the two subframes' top floor of the aseismic structure and the combined isolation structure for different ground motion cases. Figures 5 and 6 show the relative displacement response time histories in the *X*-direction and *Y*-direction of the top floor of the third subframe of the aseismic structure and the

Table 4: Subframe acceleration response and damping rate (m/s^2).

Test cases	Earthquake	Direction	Input amplitude	Floor	3rd subframe			2nd subframe		
					Aseismic	Combined isolation	Damping rate	Aseismic	Combined isolation	Damping rate
S1	Chi-Chi-2N	*Y*	0.056 g	3	1.18	0.45	61.86%	1.47	0.56	61.90%
				2	1.01	0.38	62.38%	1.16	0.49	57.76%
				1	0.69	0.32	53.62%	0.83	0.45	45.78%
S2	Chi-Chi-2F	*Y*	0.056 g	3	0.96	0.38	60.42%	1.31	0.51	61.07%
				2	0.82	0.34	58.54%	1.02	0.45	55.88%
				1	0.61	0.31	49.18%	0.67	0.40	40.30%
B1	Chi-Chi-2N	*X*	0.051 g	3	1.13	0.41	63.72%	1.42	0.48	66.20%
				2	1.02	0.37	63.73%	1.13	0.43	61.95%
				1	0.74	0.32	56.76%	0.86	0.38	55.81%
		Y	0.056 g	3	1.26	0.48	61.90%	1.59	0.58	63.52%
				2	1.05	0.45	57.14%	1.31	0.52	60.31%
				1	0.84	0.41	51.19%	0.94	0.47	50.00%
B2	Chi-Chi-2F	*X*	0.051 g	3	0.91	0.34	62.64%	1.27	0.43	66.14%
				2	0.84	0.31	63.10%	1.05	0.39	62.86%
				1	0.66	0.27	59.09%	0.69	0.36	47.83%
		Y	0.056 g	3	1.09	0.41	62.39%	1.40	0.48	65.71%
				2	0.91	0.36	60.44%	1.09	0.44	59.63%
				1	0.76	0.32	57.89%	0.78	0.38	51.28%
S3	Chi-Chi-2N	*Y*	0.153 g	3	2.62	1.02	61.07%	3.11	1.24	60.13%
				2	2.21	0.91	58.82%	2.64	1.08	59.09%
				1	1.34	0.71	47.01%	2.06	0.97	52.91%
S4	Chi-Chi-2F	*Y*	0.153 g	3	1.92	0.78	59.38%	2.76	1.03	62.68%
				2	1.60	0.63	60.63%	2.21	0.91	58.82%
				1	1.13	0.51	54.87%	1.46	0.74	49.32%
S5	Chi-Chi-3N	*Y*	0.153 g	3	3.21	1.28	60.12%	4.03	1.61	60.05%
				2	2.61	1.06	59.39%	3.57	1.51	57.70%
				1	1.73	0.91	47.40%	2.44	1.24	49.18%
B3	Chi-Chi-2N	*X*	0.140 g	3	2.41	0.87	63.90%	3.07	1.12	63.52%
				2	1.89	0.76	59.79%	2.71	1.04	61.62%
				1	1.24	0.57	54.03%	1.98	0.81	59.09%
		Y	0.153 g	3	2.86	1.06	62.94%	3.39	1.21	64.31%
				2	2.27	0.91	59.91%	2.77	1.11	59.93%
				1	1.53	0.72	52.94%	2.28	0.86	62.28%
B4	Chi-Chi-2F	*X*	0.139 g	3	1.88	0.72	61.70%	2.61	0.93	64.37%
				2	1.51	0.62	58.94%	2.13	0.81	61.97%
				1	1.04	0.43	58.65%	1.32	0.68	48.48%
		Y	0.153 g	3	2.21	0.80	63.80%	2.94	1.01	65.65%
				2	1.79	0.62	65.36%	2.38	0.86	63.87%
				1	1.36	0.49	63.97%	1.57	0.68	56.69%
B5	Chi-Chi-3N	*X*	0.113 g	3	3.02	1.12	62.91%	3.86	1.52	60.62%
				2	2.43	0.96	60.49%	3.21	1.42	55.76%
				1	1.58	0.64	59.49%	2.33	1.03	55.79%
		Y	0.153 g	3	3.44	1.30	62.21%	4.12	1.51	63.35%
				2	2.82	1.16	58.87%	3.74	1.42	62.03%
				1	1.79	0.94	47.49%	2.61	1.28	50.96%
S6	Chi-Chi-2N	*Y*	0.316 g	3	3.75	1.73	53.87%	4.72	2.01	57.42%
				2	2.51	1.56	37.85%	3.54	1.63	53.95%
				1	2.29	1.31	42.79%	2.71	1.45	46.49%
S7	Chi-Chi-2F	*Y*	0.316 g	3	3.25	1.52	53.23%	4.02	1.76	56.22%
				2	2.29	1.36	40.61%	2.98	1.52	48.99%
				1	2.08	1.22	41.35%	2.47	1.31	46.96%
S8	Chi-Chi-3N	*Y*	0.316 g	3	4.44	2.11	52.48%	5.74	2.38	58.54%
				2	3.39	1.86	45.13%	4.22	2.14	49.29%
				1	2.99	1.54	48.49%	3.37	1.63	51.63%

Table 4: Continued.

Test cases	Earthquake	Direction	Input amplitude	Floor	3rd subframe			2nd subframe		
					Aseismic	Combined isolation	Damping rate	Aseismic	Combined isolation	Damping rate
B6	Chi-Chi-2N	*X*	0.289 g	3	3.77	1.69	55.17%	4.51	1.93	57.21%
				2	2.64	1.45	45.08%	3.32	1.52	54.22%
				1	2.05	1.22	40.49%	2.74	1.34	51.09%
		Y	0.316 g	3	3.79	1.60	57.78%	5.78	2.49	56.92%
				2	2.43	1.41	41.98%	4.42	2.13	51.81%
				1	2.20	1.18	46.36%	3.39	1.88	44.54%
B7	Chi-Chi-2F	*X*	0.288 g	3	3.18	1.56	50.94%	3.81	1.61	57.74%
				2	2.05	1.31	36.10%	2.73	1.43	47.62%
				1	1.64	1.10	32.93%	2.31	1.24	46.32%
		Y	0.316 g	3	3.24	1.40	56.79%	5.12	2.16	57.81%
				2	2.47	1.27	48.58%	3.98	1.96	50.75%
				1	1.98	1.01	48.99%	2.84	1.62	42.96%
B8	Chi-Chi-3N	*X*	0.297 g	3	4.86	2.03	58.23%	5.48	2.21	59.67%
				2	3.71	1.74	53.10%	4.02	2.01	50.00%
				1	2.44	1.42	41.80%	3.32	1.62	51.20%
		Y	0.316 g	3	5.47	2.09	61.79%	6.87	2.79	59.39%
				2	3.82	1.81	52.62%	5.01	2.53	49.50%
				1	2.91	1.57	46.05%	3.78	2.04	46.03%

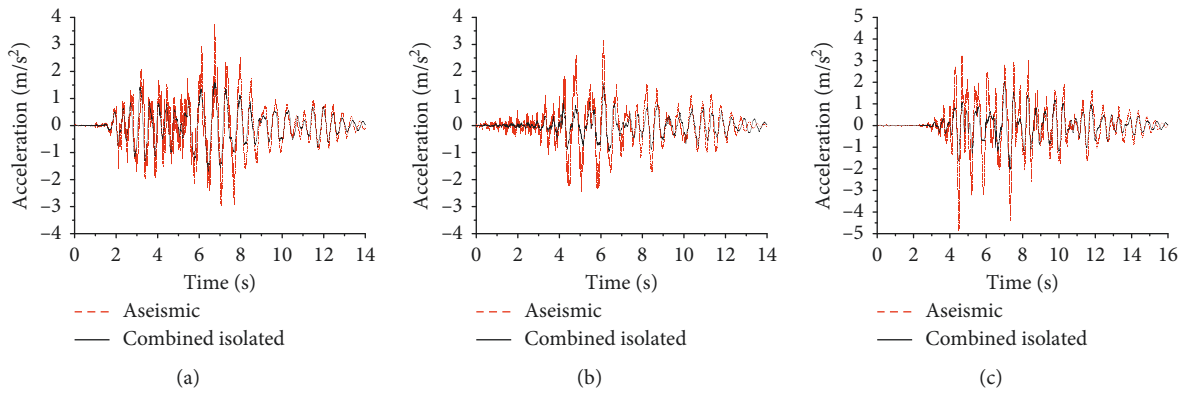

Figure 3: *X*-axis acceleration time history curves of the top floor of the third subframe. (a) Chi-Chi-2N, (b) Chi-Chi-2F, and (c) Chi-Chi-3N.

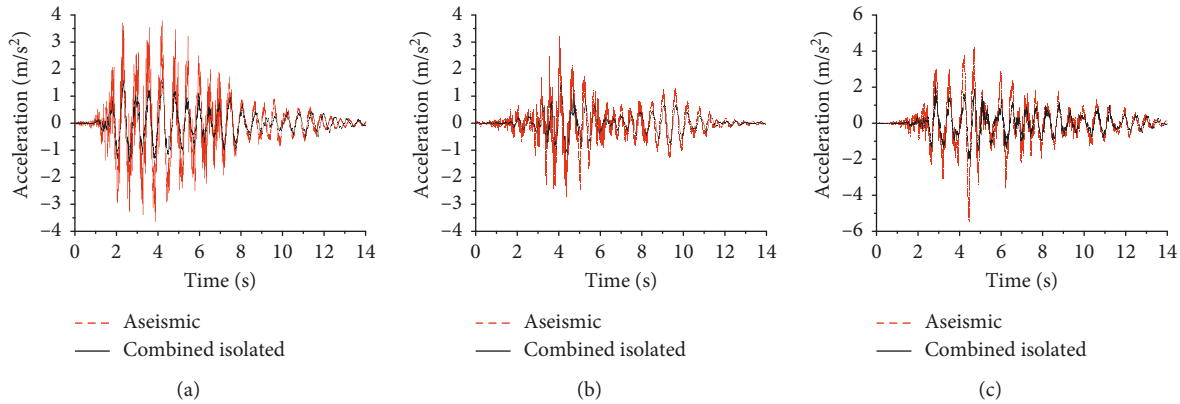

Figure 4: *Y*-axis acceleration time histories curve of the top floor of the third subframe. (a) Chi-Chi-2N, (b) Chi-Chi-2F, and (c) Chi-Chi-3N.

Table 5: Displacement response and damping rate of the subframe top floor (mm).

Test cases	Earthquake	Direction	Input amplitude	3rd subframe				2nd subframe			
				Aseismic	Combined isolation	Damping rate	Isolation layer	Aseismic	Combined isolation	Damping rate	Isolation layer
S1	Chi-Chi-2N	*Y*	0.056 g	0.84	0.3	64.29%	1.04	1.21	0.45	62.81%	0.87
S2	Chi-Chi-2F	*Y*	0.056 g	0.72	0.23	68.06%	0.86	1.04	0.4	61.54%	0.79
B1	Chi-Chi-2N	*X*	0.051 g	0.78	0.27	65.38%	1.09	1.14	0.43	62.28%	0.85
		Y	0.056 g	0.91	0.32	64.84%	1.17	1.29	0.52	59.69%	0.98
B2	Chi-Chi-2F	*X*	0.051 g	0.67	0.21	68.66%	0.83	1.01	0.35	65.35%	0.73
		Y	0.056 g	0.78	0.27	65.38%	1.01	1.08	0.41	62.04%	0.85
S3	Chi-Chi-2N	*Y*	0.153 g	2.12	0.68	67.92%	3.19	2.61	0.92	64.75%	2.73
S4	Chi-Chi-2F	*Y*	0.153 g	1.83	0.64	65.03%	2.71	2.38	0.78	67.23%	2.34
S5	Chi-Chi-3N	*Y*	0.153 g	2.55	0.88	65.49%	4.26	3.04	1.08	64.47%	3.81
B3	Chi-Chi-2N	*X*	0.140 g	1.98	0.64	67.68%	2.98	2.54	0.91	64.17%	2.56
		Y	0.153 g	2.33	0.82	64.81%	3.26	2.85	0.98	65.61%	2.82
B4	Chi-Chi-2F	*X*	0.139 g	1.76	0.54	69.32%	2.56	2.32	0.73	68.53%	2.27
		Y	0.153 g	2.01	0.67	66.67%	2.93	2.53	0.78	69.17%	2.51
B5	Chi-Chi-3N	*X*	0.113 g	2.31	0.76	67.10%	4.04	2.91	1.02	64.95%	3.64
		Y	0.153 g	2.68	0.91	66.04%	4.48	3.28	1.12	65.85%	3.94
S6	Chi-Chi-2N	*Y*	0.316 g	3.54	1.36	61.58%	6.78	4.11	1.52	63.02%	5.26
S7	Chi-Chi-2F	*Y*	0.316 g	3.09	1.04	66.34%	5.41	3.54	1.21	65.82%	4.47
S8	Chi-Chi-3N	*Y*	0.316 g	4.11	1.54	63.26%	8.24	4.56	1.64	64.04%	5.83
B6	Chi-Chi-2N	*X*	0.289 g	3.53	1.16	67.14%	6.57	3.82	1.46	61.78%	4.86
		Y	0.316 g	3.93	1.41	63.61%	6.98	4.66	1.68	63.95%	5.24
B7	Chi-Chi-2F	*X*	0.288 g	3.14	1.03	67.20%	5.07	3.64	1.24	65.93%	3.86
		Y	0.316 g	3.42	1.15	66.37%	5.42	4.13	1.27	69.25%	4.27
B8	Chi-Chi-3N	*X*	0.297 g	3.93	1.51	61.58%	7.86	4.63	1.76	61.99%	5.56
		Y	0.316 g	4.42	1.61	63.57%	8.42	5.12	1.91	62.70%	5.88

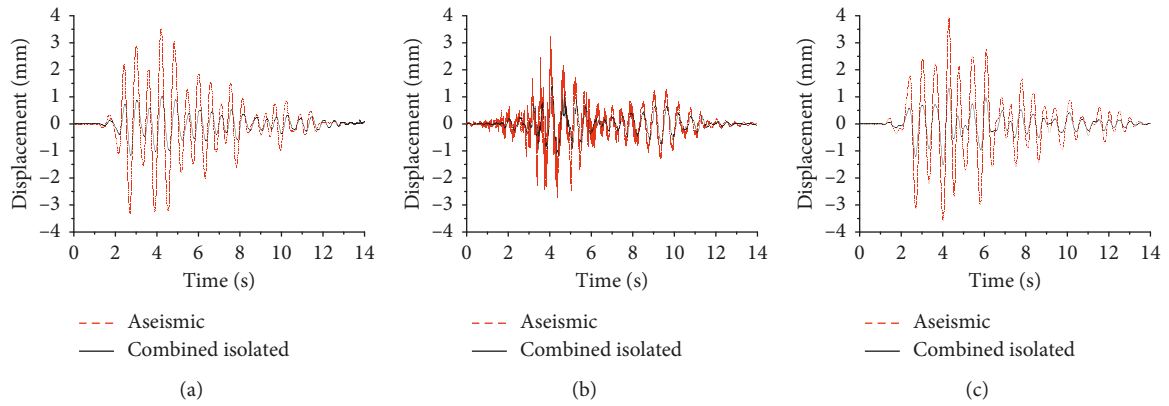

Figure 5: *X*-axis relative displacement time history curves of the top floor of the third subframe. (a) Chi-Chi-2N, (b) Chi-Chi-2F, and (c) Chi-Chi-3N.

combined isolation structure for cases B6, B7, and B8. As can be seen from Table 5 and Figures 5 and 6, the isolation layer had a significant damping effect for the displacement response of the subframe under the action of the far-fault and near-fault ground motion. This damping effect is similar to the observed acceleration response of subframes. The damping rate had a minimum of 59.69% and a maximum of 69.32% for the tested cases. The vibration reduction in both directions is similar. The displacement response of the subframe under the bidirectional earthquake was greater than that under the single-directional earthquake. The displacement response of the second subframe was greater than the third subframe. The displacement response of the subframe increases with the amplitude of the input ground motion. Due to the pulse effect, the subframe displacement response under the near-fault Chi-Chi-2N ground motion with different intensities was greater than the far-fault Chi-Chi-2F ground motion on the same site. Under near-fault

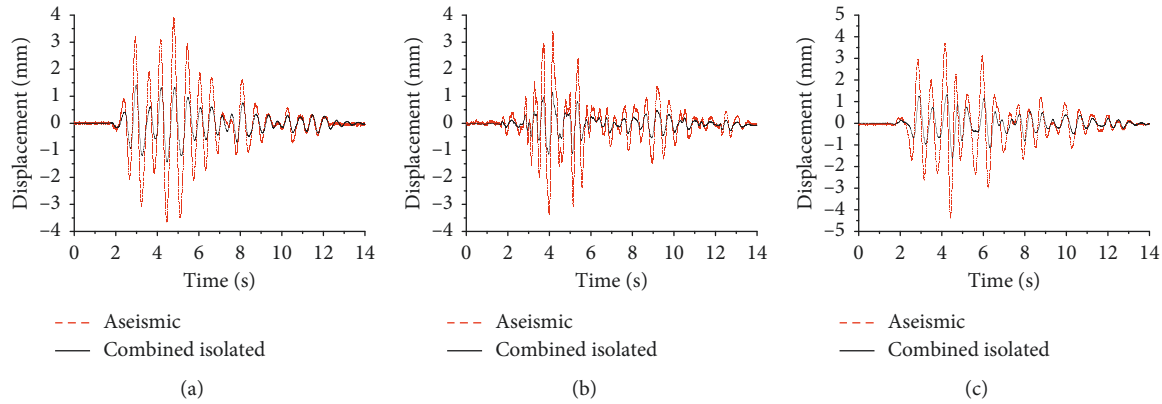

Figure 6: Y-axis relative displacement time history curves of the top floor of the third subframe. (a) Chi-Chi-2N, (b) Chi-Chi-2F, and (c) Chi-Chi-3N.

ground motion, the displacement response of the subframe was greater than the Chi-Chi-2N ground motion since the predominant period of the Chi-Chi-3N ground motion of the Class III site was closer to the basic period of the structure.

The displacement response of the isolation layer is related to the overall safety of the structure. The displacement response should be smaller than the width of the isolation joint. Table 5 provides the displacement response amplitudes of the two isolation layers under the test cases. It can be seen from Table 5 that the displacement response of the isolation layer increases as the input amplitude of ground motion increases. The displacement response of the isolation layer under the action of the Chi-Chi-2N earthquake with different intensities was greater than that of the Chi-Chi-2F earthquake, and the displacement response of the isolation layer under the Chi-Chi-3N ground motion was greater than the Chi-Chi-2N ground motion. The displacement response of the isolation layer under the action of bidirectional earthquake was greater than that of a single-directional earthquake. The maximum displacement was 8.42 mm in Y-direction, and the maximum value was 5.88 mm in X-direction. These values are both smaller than the isolation joint width of 15 mm. Therefore, on this measure at least, the structure is safe.

3.2. Main Frame Seismic Response

3.2.1. Main Frame Acceleration Response. Table 6 shows the peak value of the acceleration response and damping rate for each floor of the main frame of the aseismic structure and the combined isolation structure under the various ground motion cases. Figures 7 and 8 show the acceleration time histories and comparisons of the third floor of the main frame of the aseismic structure and the combined isolation structure in X-direction and Y-direction, respectively, for the cases of B6, B7, and B8.

It can be seen from Table 6 and Figures 7 and 8 that the acceleration response trend of the main frame and the subframe are similar. Under different ground motions, the combined isolation layer at the bottom of the subframe reduced the acceleration response of the main frame in both directions. The damping rates in both directions were similar. The damping rate had a minimum of 33.51%, and a maximum of 49.28%. The acceleration response of the main frame under a bidirectional earthquake was typically greater than that of a single-directional earthquake. The acceleration response of the main frame increased with the amplitude of the input. In the three floors, the second floor of the main frame had the smallest acceleration response. The main frame acceleration response under the Chi-Chi-2N ground motion was greater than the Chi-Chi-2F ground motion. The main frame acceleration response under the Chi-Chi-3N ground motion was greater than the Chi-Chi-2N ground motion.

The main frame plays a supporting role for the subframe, and it is the main component of the mega-substructure system to resist lateral force. Its seismic response is crucial to the safety of the overall structure. From the analysis above, it can be seen that setting the combined isolation layer at the bottom of the subframe causes the combined isolation subframe acts like a tuned mass damper on the main frame. This allows the combined isolation subframe to provide a reaction force to the main frame and reduces the acceleration response of the main frame.

3.2.2. Main Frame Displacement Response. Table 7 shows the peak value of the displacement response and the damping rate for each floor of the main frame under the various ground motion cases. Figures 9 and 10 show the displacement response time histories and comparisons of the third floor of the main frame in the X-direction and Y-direction, respectively, of the aseismic structure and the combined isolation structure for the cases of B6, B7, and B8.

It can be seen from Table 7 and Figures 9 and 10 that most of the displacement response trends of the main frame are the same as the acceleration response of the main frame. The combined isolation layer at the bottom of the subframe also reduced the displacement response of the main frame in both directions significantly. The damping rate was greater

Table 6: Main frame acceleration response and damping rate (m/s^2).

Test cases	Earthquake	Direction	Input amplitude	3rd floor			2nd floor			1st floor		
				Aseismic	Combined isolation	Damping rate	Aseismic	Combined isolation	Damping rate	Aseismic	Combined isolation	Damping rate
S1	Chi-Chi-2N	*Y*	0.056 g	1.34	0.8	40.30%	0.68	0.37	45.59%	0.82	0.46	43.90%
S2	Chi-Chi-2F	*Y*	0.056 g	1.12	0.62	44.64%	0.59	0.31	47.46%	0.72	0.45	37.50%
B1	Chi-Chi-2N	*X*	0.051 g	1.25	0.72	42.40%	0.62	0.34	45.16%	0.76	0.41	46.05%
		Y	0.056 g	1.57	0.94	40.13%	0.76	0.41	46.05%	0.88	0.46	47.73%
B2	Chi-Chi-2F	*X*	0.051 g	1.13	0.64	43.36%	0.53	0.28	47.17%	0.69	0.35	49.28%
		Y	0.056 g	1.46	0.84	42.47%	0.65	0.33	49.23%	0.76	0.4	47.37%
S3	Chi-Chi-2N	*Y*	0.153 g	3.64	2.01	44.78%	1.68	0.97	42.26%	2.49	1.46	41.37%
S4	Chi-Chi-2F	*Y*	0.153 g	3.01	1.78	40.86%	1.42	0.82	42.25%	2.13	1.18	44.60%
S5	Chi-Chi-3N	*Y*	0.153 g	4.15	2.15	48.19%	2.23	1.28	42.60%	3.08	1.83	40.58%
B3	Chi-Chi-2N	*X*	0.140 g	3.51	1.95	44.44%	1.8	1.03	42.78%	2.29	1.29	43.67%
		Y	0.153 g	3.81	2.21	41.99%	2.01	1.11	44.78%	2.64	1.53	42.05%
B4	Chi-Chi-2F	*X*	0.139 g	3.08	1.81	41.23%	1.54	0.86	44.16%	2.08	1.17	43.75%
		Y	0.153 g	3.24	1.93	40.43%	1.79	0.98	45.25%	2.29	1.28	44.10%
B5	Chi-Chi-3N	*X*	0.113 g	4.04	2.16	46.53%	2.31	1.31	43.29%	2.76	1.62	41.30%
		Y	0.153 g	4.43	2.51	43.34%	2.61	1.49	42.91%	3.17	1.87	41.01%
S6	Chi-Chi-2N	*Y*	0.316 g	5.61	3.46	38.32%	4.08	2.51	38.48%	5.09	3.21	36.94%
S7	Chi-Chi-2F	*Y*	0.316 g	5.32	3.11	41.54%	3.84	2.36	38.54%	4.46	2.87	35.65%
S8	Chi-Chi-3N	*Y*	0.316 g	7.37	4.41	40.16%	4.82	2.98	38.17%	5.46	3.54	35.16%
B6	Chi-Chi-2N	*X*	0.289 g	5.42	3.31	38.93%	3.86	2.43	37.05%	4.57	2.93	35.89%
		Y	0.316 g	7.01	4.31	38.52%	4.83	2.91	39.75%	5.52	3.67	33.51%
B7	Chi-Chi-2F	*X*	0.288 g	5.06	3.01	40.51%	3.52	2.17	38.35%	4.27	2.63	38.41%
		Y	0.316 g	6.42	3.92	38.94%	4.21	2.64	37.29%	5.01	3.21	35.93%
B8	Chi-Chi-3N	*X*	0.297 g	7.24	4.51	37.71%	4.96	3.22	35.08%	5.56	3.57	35.79%
		Y	0.316 g	8.52	5.21	38.85%	5.93	3.64	38.62%	6.96	4.37	37.21%

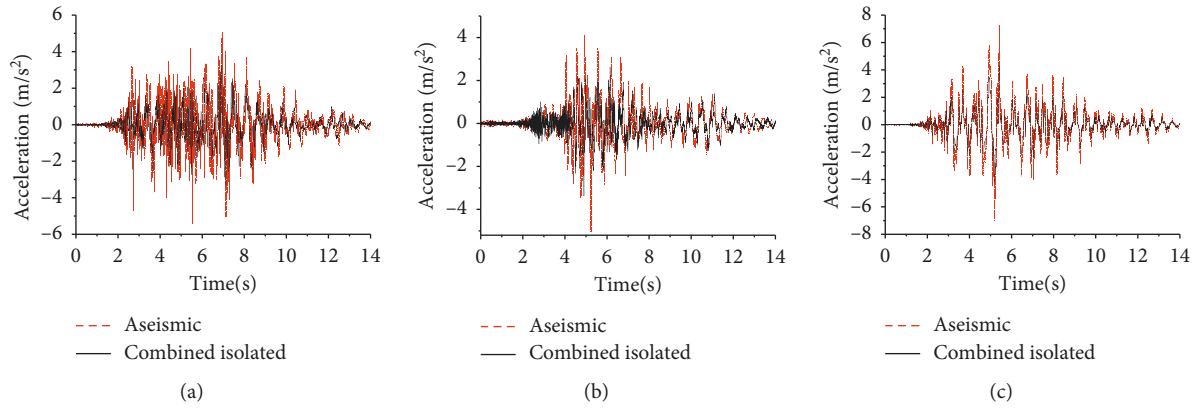

Figure 7: X-axis acceleration time history curves of the third floor of the main frame. (a) Chi-Chi-2N, (b) Chi-Chi-2F, and (c) Chi-Chi-3N.

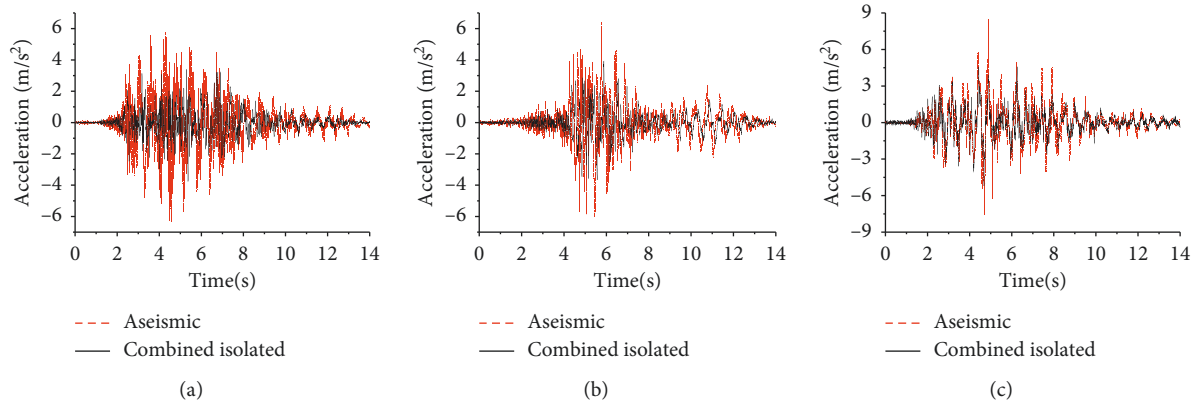

Figure 8: Y-axis acceleration time history curves of the third floor of main frame. (a) Chi-Chi-2N, (b) Chi-Chi-2F, and (c) Chi-Chi-3N.

than 25.79%, and the maximum value was 44.58%. The displacement response increased with an increase of the main frame floor level.

3.2.3. Main Frame Base Shear. Table 8 shows the shear force peak value and the damping rate of the main frame under the tested ground motion cases. The damping rate was observed to be between 32.92% and 43.10%. The base shear response of the main frame followed the same trends as the acceleration response of the main frame.

4. Conclusion

In this paper, a combined isolation layer was arranged at the joint between the bottom of the subframe and the main frame to construct a mega-substructure combined isolation system. Through comparing shaking table of the mega-subaseismic structure and the mega-subcombined isolation structure, the following conclusions are made:

(1) The combined isolation subframe acts similar to a base isolated structure for the subframe itself.

(2) The combined isolation subframe and main frame had similar damping trends of the acceleration, base shear, and displacement. However, the displacement damping rate of the subframe was significantly greater than that of the main frame significantly. The combined isolation subframe acts like a tuned mass damper for the main frame.

(3) Under the action of the far-fault and near-fault ground motions, the isolation layer had a significant damping effect on the acceleration and displacement response of all subframes in both directions. The damping effect was stronger on the displacement than the acceleration, and the damping effects in the two directions are similar.

(4) The seismic response of the subframe under the bidirectional earthquake was greater than that under the single-directional earthquake.

(5) The seismic response of the subframe increased with the amplitude of the ground motion input.

(6) The seismic response of the second subframe was greater than the third subframe.

(7) The pulse effect increased the seismic response of the structure, and so the increase of the predominant period of ground motion also increased the seismic response of the structure.

Table 7: Main frame displacement response and damping rate (mm).

Test cases	Earthquake	Direction	Input amplitude	3rd floor			2nd floor			1st floor		
				Aseismic	Combined isolation	Damping rate	Aseismic	Combined isolation	Damping rate	Aseismic	Combined isolation	Damping rate
S1	Chi-Chi-2N	*Y*	0.056 g	2.21	1.38	37.56%	1.32	0.84	36.36%	0.88	0.51	42.05%
S2	Chi-Chi-2F	*Y*	0.056 g	1.9	1.22	35.79%	1.06	0.63	40.57%	0.71	0.43	39.44%
B1	Chi-Chi-2N	*X*	0.051 g	2.33	1.53	34.33%	1.22	0.77	36.89%	0.78	0.45	42.31%
		Y	0.056 g	2.43	1.62	33.33%	1.38	0.86	37.68%	0.83	0.46	44.58%
B2	Chi-Chi-2F	*X*	0.051 g	1.95	1.22	37.44%	1.02	0.61	40.2%	0.64	0.37	42.19%
		Y	0.056 g	1.97	1.24	37.06%	1.12	0.65	41.96%	0.68	0.41	39.71%
S3	Chi-Chi-2N	*Y*	0.153 g	4.86	3.11	36.01%	3.54	2.04	42.37%	2.37	1.37	42.19%
S4	Chi-Chi-2F	*Y*	0.153 g	4.31	2.67	38.05%	3.02	1.81	40.07%	1.96	1.18	39.8%
S5	Chi-Chi-3N	*Y*	0.153 g	6.62	4.12	37.76%	4.42	2.51	43.21%	2.94	1.74	40.82%
B3	Chi-Chi-2N	*X*	0.140 g	4.63	3.02	34.77%	3.28	1.97	39.94%	2.21	1.32	40.27%
		Y	0.153 g	5.22	3.47	33.52%	3.69	2.17	41.19%	2.49	1.53	38.55%
B4	Chi-Chi-2F	*X*	0.139 g	4.11	2.51	38.93%	2.81	1.76	37.37%	1.84	1.14	38.04%
		Y	0.153 g	4.61	2.98	35.36%	3.15	1.91	39.37%	2.13	1.31	38.5%
B5	Chi-Chi-3N	*X*	0.113 g	6.65	4.28	35.64%	3.87	2.29	40.83%	2.78	1.65	40.65%
		Y	0.153 g	6.87	4.46	35.08%	4.56	2.61	42.76%	3.08	1.91	37.99%
S6	Chi-Chi-2N	*Y*	0.316 g	8.83	6.02	31.82%	6.22	3.72	40.19%	3.86	2.44	36.79%
S7	Chi-Chi-2F	*Y*	0.316 g	7.56	5.61	25.79%	5.26	3.55	32.51%	3.21	2.28	28.97%
S8	Chi-Chi-3N	*Y*	0.316 g	11.46	7.63	33.42%	7.02	4.52	35.61%	4.42	2.78	37.10%
B6	Chi-Chi-2N	*X*	0.289 g	9.34	6.08	34.90%	6.42	4.36	32.09%	3.12	2.21	29.17%
		Y	0.316 g	8.42	5.08	39.67%	6.02	4.16	30.90%	3.02	2.01	33.44%
B7	Chi-Chi-2F	*X*	0.288 g	7.92	5.53	30.18%	5.54	3.81	31.23%	2.61	1.87	28.35%
		Y	0.316 g	7.17	4.61	35.70%	5.23	3.74	28.49%	2.48	1.72	30.65%
B8	Chi-Chi-3N	*X*	0.297 g	11.58	7.44	35.75%	7.12	4.66	34.55%	3.69	2.66	27.91%
		Y	0.316 g	13.02	7.84	39.78%	7.02	4.75	32.34%	3.78	2.45	35.19%

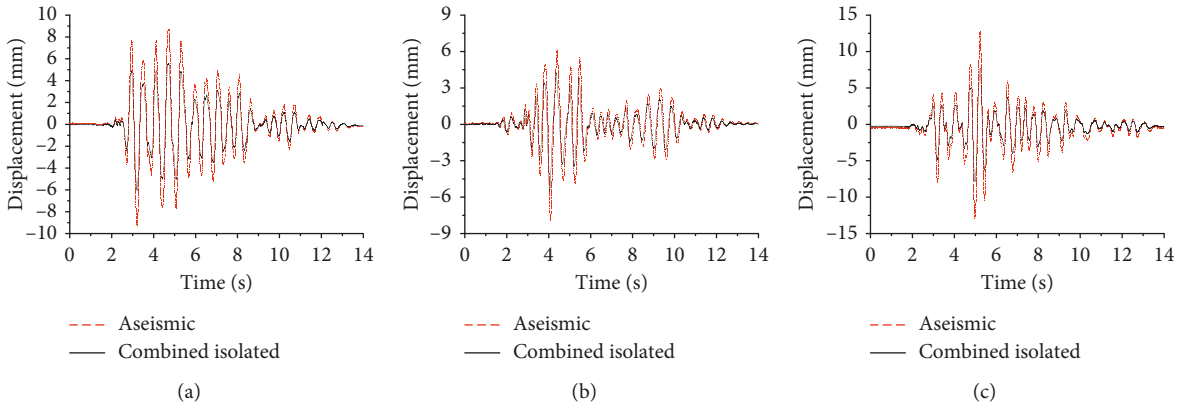

Figure 9: *X*-axis relative displacement time history curves of the third floor of main frame. (a) Chi-Chi-2N, (b) Chi-Chi-2F, and (c) Chi-Chi-3N.

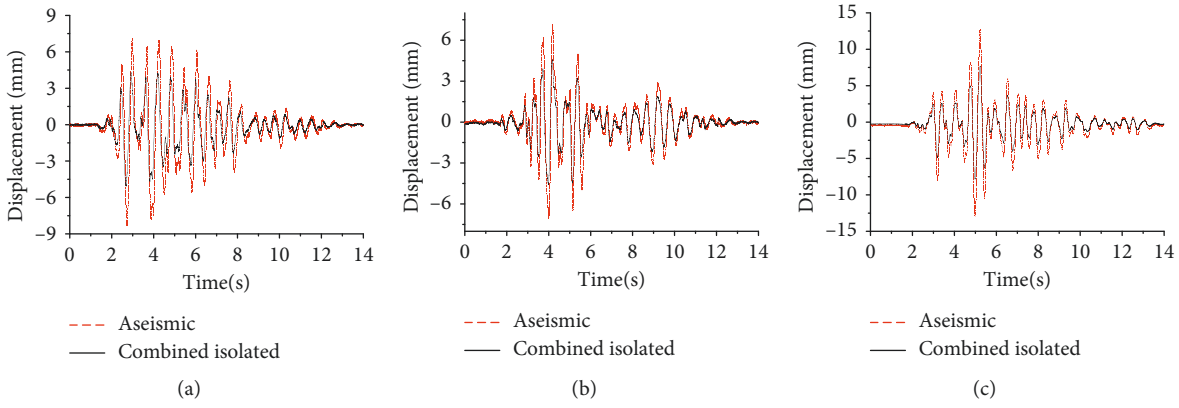

Figure 10: *Y*-axis relative displacement time history curves of the third floor of main frame. (a) Chi-Chi-2N, (b) Chi-Chi-2F, and (c) Chi-Chi-3N.

Table 8: Main frame base shear response and damping rate (kN).

Test cases	Earthquake	Direction	Input amplitude	Aseismic	Combined isolation	Damping rate
S1	Chi-Chi-2N	*Y*	0.056 g	3.44	2.03	40.99%
S2	Chi-Chi-2F	*Y*	0.056 g	2.86	1.76	38.46%
B1	Chi-Chi-2N	*X*	0.051 g	3.48	1.98	43.10%
		Y	0.056 g	3.62	2.07	42.82%
B2	Chi-Chi-2F	*X*	0.051 g	2.97	1.76	40.74%
		Y	0.056 g	3.11	1.87	39.87%
S3	Chi-Chi-2N	*Y*	0.153 g	9.38	5.83	37.85%
S4	Chi-Chi-2F	*Y*	0.153 g	8.14	5.02	38.33%
S5	Chi-Chi-3N	*Y*	0.153 g	11.46	6.84	40.31%
B3	Chi-Chi-2N	*X*	0.140 g	9.12	5.61	38.49%
		Y	0.153 g	9.87	6.12	37.99%
B4	Chi-Chi-2F	*X*	0.139 g	8.01	4.87	39.20%
		Y	0.153 g	8.64	5.31	38.54%
B5	Chi-Chi-3N	*X*	0.113 g	11.16	6.69	40.05%
		Y	0.153 g	12.13	7.24	40.31%
S6	Chi-Chi-2N	*Y*	0.316 g	16.42	9.98	39.22%
S7	Chi-Chi-2F	*Y*	0.316 g	14.15	8.69	38.59%
S8	Chi-Chi-3N	*Y*	0.316 g	18.49	11.87	35.80%
B6	Chi-Chi-2N	*X*	0.289 g	16.91	10.4	38.50%
		Y	0.316 g	17.43	10.7	38.61%
B7	Chi-Chi-2F	*X*	0.288 g	14.67	9.84	32.92%
		Y	0.316 g	14.88	9.75	34.48%
B8	Chi-Chi-3N	*X*	0.297 g	19.69	11.75	40.33%
		Y	0.316 g	19.96	11.98	39.98%

(8) The displacement response of the isolation layer was less than the width of the isolation joint, which ensures the safety of the structure.

Data Availability

The data used to support the findings of this study are available from the corresponding author upon request.

Conflicts of Interest

The authors declare that they have no conflicts of interest.

Acknowledgments

The authors acknowledge the support from National Natural Science Foundation of China (Grant no. 51578160), Science and Technology Project of Fujian Education Department (Grant no. JA15050), and Fujian Science and Technology Plan Project (Grant no. 2018Y0057).

References

[1] E. Brunesi, R. Nascimbene, and L. Casagrande, "Seismic analysis of high-rise mega-braced frame-core buildings," *Engineering Structures*, vol. 115, pp. 1–17, 2016.

[2] X. Lu, L. Xie, C. Yu, and X. Lu, "Development and application of a simplified model for the design of a super-tall mega-braced frame-core tube building," *Engineering Structures*, vol. 110, pp. 116–126, 2016.

[3] X. Lu, Y. Zou, W. Lu, and B. Zhao, "Shaking table model test on shanghai world financial center tower," *Earthquake Engineering & Structural Dynamics*, vol. 36, no. 4, pp. 439–457, 2007.

[4] M. Cheng and X. Lu, "Study on seismic behaviour of a new hybrid structure with shaking table test and numerical analysis," *The Structural Design of Tall and Special Buildings*, vol. 19, no. 7, pp. 750–760, 2010.

[5] J. Kim and M. Jung, "Progressive collapse-resisting capacity of modular mega-frame buildings," *Structural Design of Tall and Special Buildings*, vol. 22, no. 6, pp. 471–484, 2013.

[6] A. A. Markou, G. Stefanou, and G. D. Manolis, "Stochastic energy measures for hybrid base isolation systems," *Soil Dynamics and Earthquake Engineering*, 2018.

[7] M. Q. Feng, "Application of hybrid sliding isolation system to buildings," *Journal of Engineering Mechanics*, vol. 119, no. 10, pp. 2090–2108, 1993.

[8] S. P. Chang, N. Makris, A. S. Whittaker, and A. C. T. Thompson, "Experimental and analytical studies on the performance of hybrid isolation systems," *Earthquake Engineering and Structural Dynamics*, vol. 31, no. 2, pp. 421–443, 2002.

[9] G. Oliveto, N. D. Oliveto, and A. Athanasiou, "Constrained optimization for 1-D dynamic and earthquake response analysis of hybrid base-isolation systems," *Soil Dynamics and Earthquake Engineering*, vol. 67, pp. 44–53, 2014.

[10] M. K. Shrimali and R. S. Jangid, "Non-linear seismic response of base-isolated liquid storage tanks to bi-directional excitation," *Nuclear Engineering and Design*, vol. 217, no. 1-2, pp. 1–20, 2002.

[11] A. B. M. S. Islam, R. R. Hussain, M. Jameel et al., "Non-linear time domain analysis of base isolated multi-storey building under site specific bi-directional seismic loading," *Automation in Construction*, vol. 22, pp. 554–566, 2012.

[12] D. Cancellara and F. De Angelis, "Nonlinear dynamic analysis for multi-storey RC structures with hybrid base isolation systems in presence of bi-directional ground motions," *Composite Structures*, vol. 154, pp. 464–492, 2016.

[13] S. Bhagat and A. C. Wijeyewickrema, "Seismic response evaluation of base-isolated reinforced concrete buildings under bidirectional excitation," *Earthquake Engineering and Engineering Vibration*, vol. 16, no. 2, pp. 365–382, 2017.

[14] Y. Shi, M. Kurata, and M. Nakashima, "Disorder and damage of base-isolated medical facilities when subjected to near-fault and long-period ground motions," *Earthquake Engineering & Structural Dynamics*, vol. 43, no. 11, pp. 1683–1701, 2014.

[15] V. Calugaru and M. Panagiotou, "Seismic response of 20-story base-isolated and fixed-base reinforced concrete structural wall buildings at a near-fault site," *Earthquake Engineering & Structural Dynamics*, vol. 43, no. 6, pp. 927–948, 2014.

[16] C. P. Providakis, "Pushover analysis of base-isolated steel–concrete composite structures under near-fault excitations," *Soil Dynamics and Earthquake Engineering*, vol. 28, no. 4, pp. 293–304, 2008.

[17] F. Mazza and A. Vulcano, "Effects of near-fault ground motions on the nonlinear dynamic response of base-isolated rc framed buildings," *Earthquake Engineering & Structural Dynamics*, vol. 41, no. 2, pp. 211–232, 2012.

[18] C. Alhan, H. Gazi, and H. Kurtuluş, "Significance of stiffening of high damping rubber bearings on the response of base-isolated buildings under near-fault earthquakes," *Mechanical Systems and Signal Processing*, vol. 79, pp. 297–313, 2016.

[19] Y. Zhang and W. D. Iwan, "Protecting base-isolated structures from near-field ground motion by tuned interaction damper," *Journal of Engineering Mechanics*, vol. 128, no. 3, pp. 287–295, 2002.

[20] S. Gur, S. K. Mishra, and S. Chakraborty, "Performance assessment of buildings isolated by shape-memory-alloy rubber bearing: comparison with elastomeric bearing under near-fault earthquakes," *Structural Control and Health Monitoring*, vol. 21, no. 4, pp. 449–465, 2014.

[21] B. Mehrparvar and F. Khoshnoudian, "Efficiency of active systems in controlling base-isolated buildings subjected to near-fault earthquakes," *The Structural Design of Tall and Special Buildings*, vol. 20, no. 8, pp. 1019–1034, 2011.

[22] M. Q. Feng and A. Mita, "Vibration control of tall buildings using mega subconfiguration," *Journal of Engineering Mechanics*, vol. 121, no. 10, pp. 1082–1088, 1995.

[23] W. Chai and M. Q. Feng, "Vibration control of super tall buildings subjected to wind loads," *International Journal of Non-Linear Mechanics*, vol. 32, no. 4, pp. 657–668, 1997.

[24] Z. Lan, Y. Tian, L. Fang, S. Liang, and X. Wang, "An experimental study on seismic responses of multifunctional vibration-absorption reinforced concrete megaframe structures," *Earthquake Engineering & Structural Dynamics*, vol. 33, no. 1, pp. 1–14, 2004.

[25] Z. Xun'an, W. Dong, and J. Jiesheng, "The controlling mechanism and the controlling effectiveness of passive mega-sub-controlled frame subjected to random wind loads," *Journal of Sound and Vibration*, vol. 283, no. 3–5, pp. 543–560, 2005.

[26] Y. Lian, X. Zhang, and C. Sheldon, "Damping characteristics of friction damped braced frame and its effectiveness in the mega-sub controlled structure system," *Earthquake Engineering and Engineering Vibration*, vol. 6, no. 2, pp. 171–181, 2007.

[27] X. Zhang, X. Qin, S. Cherry, Y. Lian, J. Zhang, and J. Jiang, "A new proposed passive mega-sub controlled structure and response control," *Journal of Earthquake Engineering*, vol. 13, no. 2, pp. 252–274, 2009.

[28] X. Li, P. Tan, X. Li, and A. Liu, "Seismic performance evaluations of mega-sub isolation system," *Mathematical Problems in Engineering*, vol. 2016, Article ID 7031712, 16 pages, 2016.

[29] P. Tan, Y. Zhang, X. Li, X. Li, A. Liu, and F. Zhou, "Experimental investigation of mega-sub isolation structure," *The Structural Design of Tall and Special Buildings*, vol. 26, no. 16, p. e1360, 2017.